Recurrent processing drives experience-dependent plasticity for perceptual decisions

Ke Jia[1], Elisa Zamboni[1], Valentin Kemper[3], Catarina Rua[2], Nuno Reis Goncalves[1], Adrian Ka Tsun Ng[1,4] Christopher T. Rodgers[2], Guy Williams[2], Rainer Goebel[3] and Zoe Kourtzi[1,*]

[1]Department of Psychology, University of Cambridge, Cambridge, CB2 3EB, UK.

[2]Wolfson Brain Imaging Centre, Department of Clinical Neurosciences, University of Cambridge, Cambridge, CB2 0QQ, UK.

[3]Department of Cognitive Neuroscience, Faculty of Psychology and Neuroscience, Maastricht University, Maastricht, 6200 MD, The Netherlands.

[4]Department of Industrial and Manufacturing Systems Engineering, The University of Hong Kong, Hong Kong SAR, China.

Correspondence:

Zoe Kourtzi

Department of Psychology

University of Cambridge

Cambridge, UK

Email: zk240@cam.ac.uk

Abstract

Learning and experience are critical for translating ambiguous sensory information from our environments to perceptual decisions. Yet, evidence on how training molds the adult human brain remains controversial, as fMRI at standard resolution does not allow us to discern the finer-scale mechanisms that underlie sensory plasticity. Here, we combine ultra-high field (7T) functional imaging at sub-millimetre resolution with orientation discrimination training to interrogate experience-dependent plasticity across cortical depths. Our results provide evidence for recurrent plasticity, by contrast to sensory encoding vs. feedback mechanisms. We demonstrate that learning alters orientation-specific representations in superficial rather than middle V1 layers, suggesting changes in read-out rather than input signals. Further, learning increases feedforward rather than feedback layer-to-layer connectivity in occipito-parietal regions, suggesting that sensory plasticity gates perceptual decisions. Our findings propose finer-scale plasticity mechanisms that re-weight sensory signals to inform improved decisions, bridging the gap between micro- and macro- circuits of experience-dependent plasticity.

Keywords

ultra-high field brain imaging, learning, experience-dependent plasticity, perceptual decisions, visual cortex

Introduction

Understanding the world around us depends on the brain resolving ambiguous information from our senses to inform our decisions and actions. The brain learns to interpret sensory signals by using past experience to optimize perceptual judgments. Although this experience-dependent brain plasticity is most evident during development, training in adulthood is shown to improve visual recognition skills and alter the brain's function and connectivity[1–4]. Yet, evidence on how practice molds the adult human brain and results in improved decisions remains controversial.

The neural computations that mediate experience-dependent plasticity are highly debated (e.g. [1,5,6]). Results from behavioral training studies focusing on visual discrimination tasks (i.e. perceptual learning tasks) have long been understood to suggest that plasticity occurs at early stages of sensory processing (i.e. primary visual cortex), as learning was shown to be specific to the trained stimulus features (e.g. [7,8]). Neurophysiological recordings[9,10] and human imaging data [11–13] support this early neural locus hypothesis by showing that training changes neural responses in primary visual cortex, implying that learning alters stimulus encoding. By contrast, other studies have shown that learning alters processing in higher visual areas[14,15] and regions involved in decision-making[6,16]. This suggests that learning changes the read-out of sensory information[5] from higher cortical areas rather than sensory encoding in visual cortex, with changes in activity in early visual cortex reflecting feedback processes[17].

Here, we capitalize on recent advances in brain imaging technology (i.e. Ultra-High Field: UHF imaging) that allow us to interrogate brain computations at a finer scale than that afforded by standard fMRI techniques[18]. UHF imaging affords the sub-millimetre resolution necessary to examine fMRI signals across cortical laminar layers that are known to be associated with dissociable brain computations (Figure 1). In particular, sensory input is known to enter the

cortex from the thalamus at the level of the middle layer (layer 4) and output information is fed forward from the superficial layers (layer 2/3), while feedback information is exchanged primarily between deeper (layer 5/6) and superficial layers[19–22]. Further, horizontal connections across V1 columns are known to predominantly terminate in superficial layers[23,24] and suggested to support recurrent processing within visual cortex[25,26]. Neurophysiological studies have shown that this micro-circuit is involved in a range of visual recognition[26] and attention[27] tasks. Recent laminar fMRI studies provide evidence for the involvement of this circuit in the context of sensory processing[28] and visual attention[29].

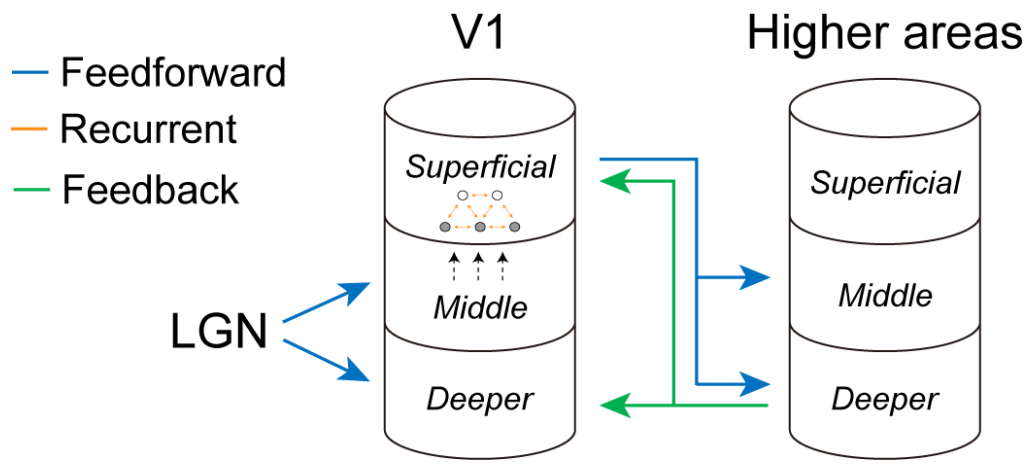

Figure 1. Laminar brain circuits.

Schematic representation of the hypotheses tested, training may modify: a) feedforward processing (blue arrows) between LGN and V1; b) recurrent processing via horizontal connections within the visual cortex (horizontal connections (indicated by orange arrows) between excitatory (open circles) and inhibitory (filled circles) neurons adapted from Teich et al. (2003) and Schwabe et al. (2005)); c) feedback processing (green arrows) between V1 and higher areas (i.e., V2, V3, V4, IPS) based on known anatomical circuits.

We combine 7T laminar fMRI (i.e. before and after training) with training on an orientation discrimination task, to test whether learning modifies: a) encoding of sensory input in middle V1 layers, b) recurrent processing in superficial layers that alters the sensory read-out, c) feedback processing in deeper or superficial V1 layers from higher decision-related regions (i.e. intra-parietal cortex, IPS). Using multi-voxel pattern classification analysis (MVPA) across cortical depths, we demonstrate learning-dependent changes in visual representations that are specific to superficial rather than middle or deeper V1 layers, suggesting that learning modifies read-out rather than input signals in visual cortex. Further, we show enhanced feedforward connectivity between superficial layers in visual cortex and middle layers of posterior parietal cortex, rather than feedback connectivity between deeper layers in these areas. Our findings offer an alternate proposal to the ongoing debate focusing on encoding vs. feedback mechanisms of experience-dependent plasticity: learning is implemented by recurrent computations that alter read-out rather than sensory encoding in visual cortex and feedforward processing from sensory to decision related areas.

Results

Learning-dependent changes in perceptual discrimination

We trained participants (N = 15; data from two participants were excluded due to excessive head movement and technical issues during acquisition) on an orientation discrimination task[9,12] for five consecutive days and tested their performance on the same task during fMRI scanning before and after training (Figure 2A&B). Participants' discrimination performance improved during training (Figure 2C), as indicated by a significant decrease in threshold (~79.4%) performance (paired t-test, mean threshold on day 1 vs. day 5: $t(12) = 8.108$, $p < 0.001$).

To determine the specificity of this learning, we measured participants' discrimination threshold for two different orientations (i.e., trained vs. untrained orientations that corresponded to 55° or 125°) at two different locations (i.e., trained vs. untrained location that corresponded to the left or right visual field) before and after training. Our results showed that behavioral improvement due to training was stronger for the trained orientation and location (Figure 2D, Figure S1), consistent with previous studies[8] showing specificity to the trained stimulus features. In particular, we observed a significant orientation × location × session interaction (repeated measures ANOVA, $F(1,12) = 11.858$, $p = 0.005$) and a significant orientation × session interaction ($F(1,12) = 21.551$, $p = 0.001$) at the trained, but not the untrained ($F(1,12) = 3.093$, $p = 0.104$) location. As suggested by recent work[7], it is likely that this learning specificity is due to prolonged training near threshold (i.e. employing a single staircase[30]), in contrast to supra-threshold training that has been suggested to enhance transfer and higher-level learning[31].

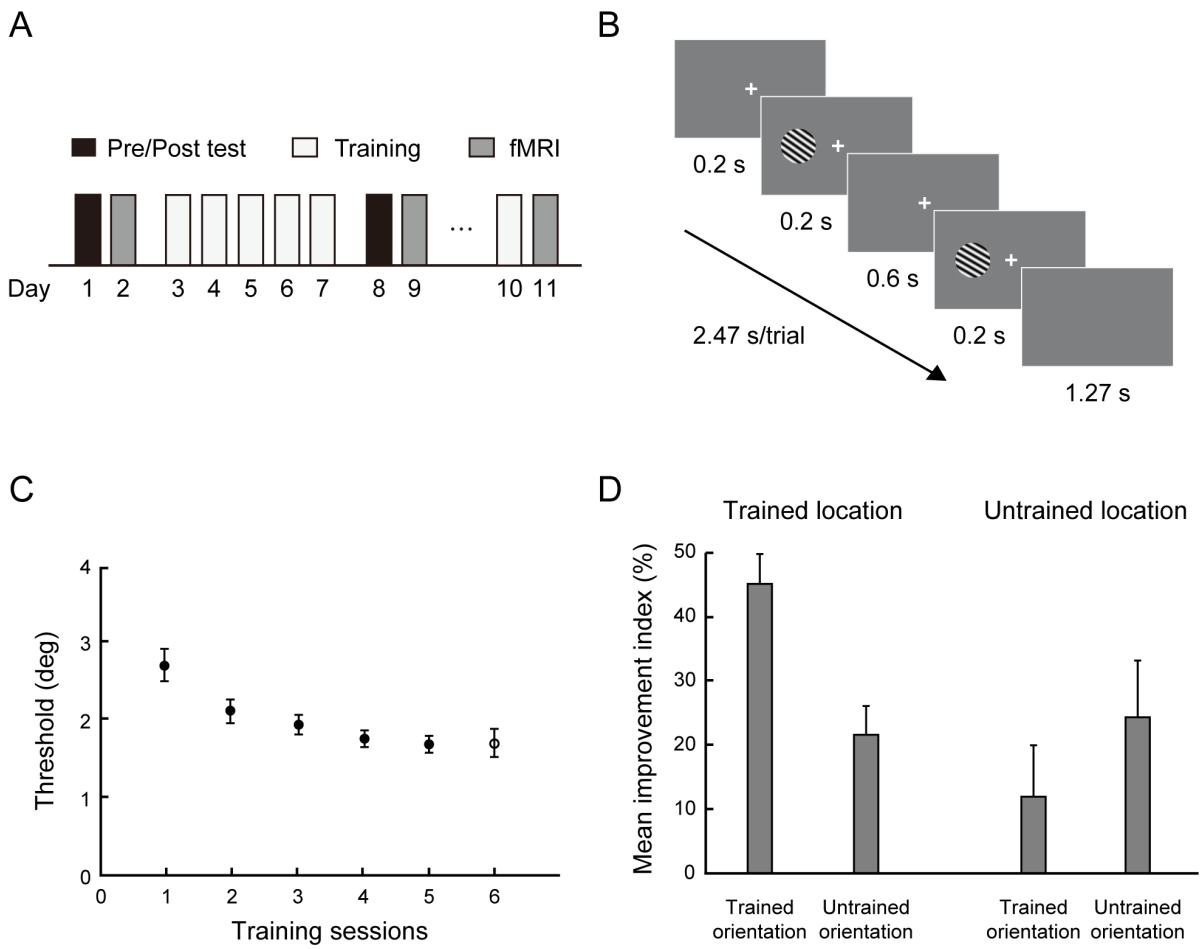

Figure 2. Experimental design, task and behavioral results.

(A) Experimental design. Participants were trained on an orientation discrimination task with feedback for five consecutive days. Before and after training, we measured participant's performance on the same task without feedback in the lab and during scanning. (B) Orientation discrimination task. For each trial, participants were asked to report whether the second grating was tilted clockwise or counterclockwise relative to the first grating. (C) Mean performance across participants at 79.4% threshold for the training (filled circles) and the control (open circle) sessions. (D) Mean improvement index (MPI = (pre-test threshold – post-test threshold) / pre-test threshold × 100%) showed learning specificity for the trained compared to the untrained orientation presented at the trained vs. untrained location. A two-way repeated measures ANOVA on MPI (orientation × location) showed a significant interaction ($F(1,12) = 14.847$, $p = 0.002$). Post-hoc comparisons showed significantly higher improvement for the trained than the

untrained ($t(12) = 5.564$, $p < 0.001$) orientation at the trained location. In contrast, no significant differences were observed between the trained and the untrained ($t(12) = -1.608$, $p = 0.134$) orientations at the untrained location. Error bars indicate standard error of the mean across participants.

Learning-dependent changes across cortical depth in the visual cortex

To test whether learning alters orientation representations across cortical depth in the visual cortex, we segmented the visual areas and assigned voxels to three layers (superficial, middle, deeper) using an equi-volume approach (*see Methods, Anatomical data analyses for details*; Figure 3A-D). We used MVPA to discern orientation-specific fMRI signals and test for differences in these signals before vs. after training across layers. In particular, we tested whether linear classifiers that were trained on fMRI signals from multi-voxel patterns in different V1 layers (superficial, middle, deeper) discriminated between: a) trained (55° or 125°) vs. control (vertical) orientations, b) untrained (125° or 55°) vs. control (vertical) orientations. Classifying each of the reference orientations (55° or 125°) from the control (vertical) orientation allowed us to test learning-dependent changes separately for the trained vs. untrained orientations. We hypothesized that higher MVPA accuracy after training for the trained vs. control orientation classification than the untrained vs. control orientation classification would indicate orientation-specific learning-dependent plasticity. Note that, as both the trained and untrained orientation differed equally from the control orientation (~55°), accuracy differences between these classification tasks could not be attributed to stimulus differences.

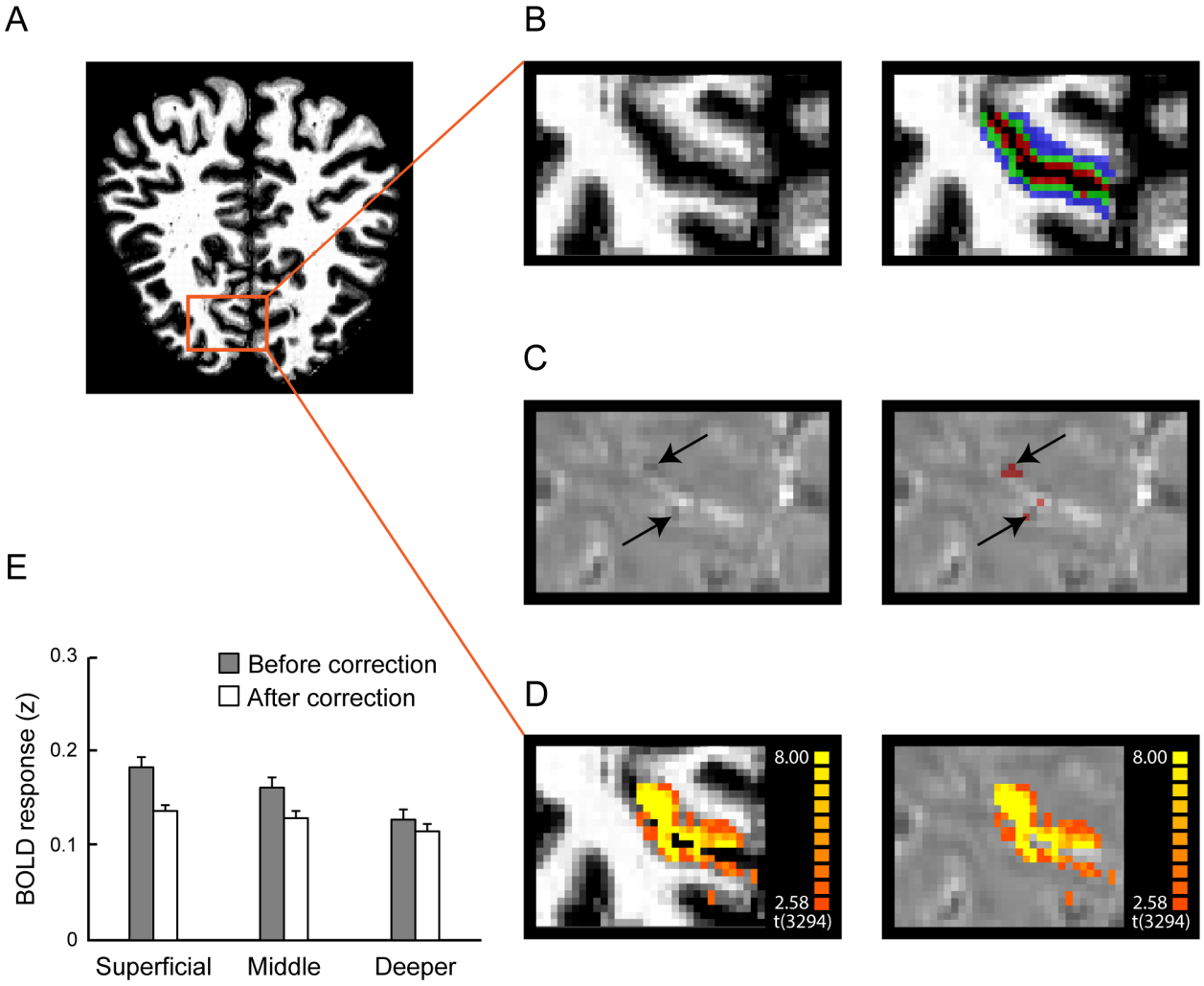

Figure 3. fMRI layer definition and vascular correction.

(A) Coronal view of the anatomical image of a sample participant. Red insert indicates region of interest in visual cortex. (B) Layers definition map overlaid on an anatomical image (blue: deeper layers, green: middle layers, and red: superficial layers). (C) Voxels confounded by vasculature-related effects (highlighted by arrows and in red) overlaid on functional images. (D) BOLD activation map (stimulus vs. fixation) overlaid on the anatomical (left panel) and functional data (right panel). (E) Mean normalized BOLD in V1 before and after correction for vasculature-related effects, showing reduced superficial bias after correction. Error bars indicate standard error of the mean across participants. We observed significant interactions (pre-test session: $F(2,24) = 50.961$, $p < 0.001$, post-test session: $F(2,24) = 36.887$,

$p < 0.001$) between layer (superficial, middle, deeper) and BOLD signal (before vs. after correction). The stronger BOLD decrease in upper (i.e. superficial, middle) than deeper layers after correction suggests that our approach for correcting vasculature-related effects controlled substantially for the superficial bias.

Our results showed learning-dependent changes (i.e. increased MVPA accuracy) for the trained orientation in superficial rather than middle or deeper layers in V1 (Figure 4, Figure 5A). In particular, a three-way repeated measures ANOVA (orientation × session × layer) on the MVPA accuracy showed a significant three-way interaction ($F(2,24) = 4.244$, $p = 0.026$). Two-way repeated measures ANOVAs (orientation × session) showed a significant interaction in superficial V1 layers ($F(1,12) = 12.223$, $p = 0.004$), but not in middle ($F(1,12) = 0.012$, $p = 0.913$), nor deeper ($F(1,12) = 0.446$, $p = 0.517$) layers. Further, we observed enhanced discriminability (i.e. MVPA accuracy) for the trained orientation in superficial ($t(12) = -2.665$, $p = 0.021$), but not middle ($t(12) = -0.783$, $p = 0.449$), nor deeper ($t(12) = -0.489$, $p = 0.633$) layers. In contrast, we did not observe any significant learning-dependent changes for orientations presented in the untrained location. In particular, there was no significant three-way interaction (orientation × session × layer, $F(2,24) = 0.603$, $p = 0.555$) nor any significant orientation × session interactions across V1 layers (superficial layers: $F(1,12) = 0.053$, $p = 0.821$; middle layers: $F(1,12) = 0.538$, $p = 0.478$; deeper layers: $F(1,12) = 2.211$, $p = 0.163$). Taken together, our results showed that learning-dependent changes in orientation representations in superficial V1 layers were specific to the trained orientation and location. It is unlikely that these learning-dependent changes in visual representations were due to differences in attention related to task difficulty before vs. after training, as participant performance was matched across scanning sessions.

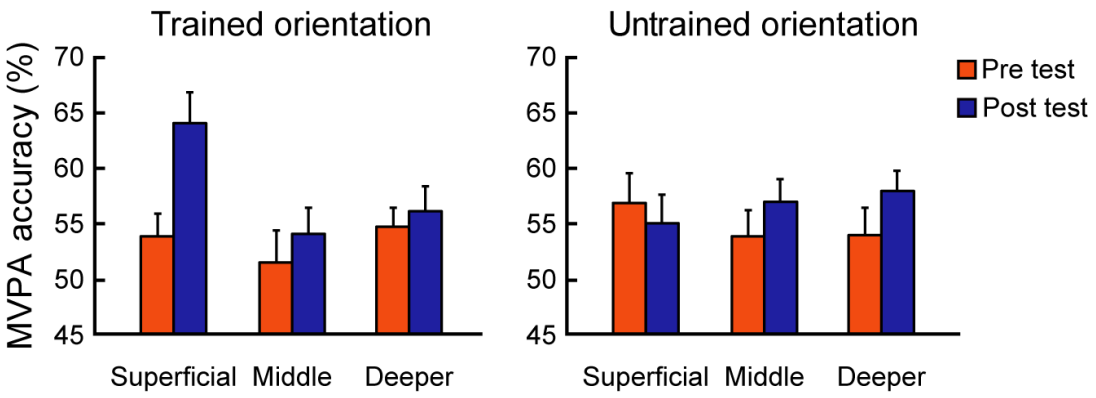

Figure 4. MVPA results before and after training across V1 layers.

MVPA accuracy across V1 layers for the trained and untrained orientations presented at the trained location. To further validate our classification results, we trained the classifier after shuffling the labels of the training data set for 5000 times. This analysis returned classification accuracies that did not differ significantly from chance (all *ps* > 0.618, FDR corrected), suggesting that our MVPA analysis extracted reliable voxel pattern information from the ROIs tested. Error bars indicate standard error of the mean across participants.

Complementary and control analyses

To further validate our results and control for potential confounds we conducted the following additional analyses.

First, it has been shown that the overall BOLD signal as measured by GE-EPI is higher at the cortical surface due to vascular contributions[32] resulting in loss of spatial specificity[33]. Here, we combined several approaches to reduce this superficial bias by removing voxels with low temporal signal to noise ratio and high t-statistic for stimulation contrast (*see Methods, correcting for vascular effects for details*). We then z-scored each voxel's time course to account for possible differences in signal strength and variance due to thermal or physiological noise across layers while preserving differences between conditions[29]. These corrections resulted in

203 similar BOLD magnitude and multi-voxel pattern classification accuracy before training across
204 layers (Figure 3E), suggesting that our approach for correcting vasculature-related effects
205 controlled substantially for the superficial bias. In particular, consistent with previous studies[34]
206 showing reduced superficial bias for MVPA classification measures, we did not observe any
207 significant differences in MVPA accuracy between trained and untrained orientations before
208 training (e.g. orientation × location × layer interaction: $F(2,24) = 0.891$, $p = 0.423$; main effect
209 of layer: $F(2,24) = 0.287$, $p = 0.753$). Thus, it is unlikely that our MVPA results after vasculature
210 correction were significantly confounded by the superficial bias.

211 Second, we applied a spatial regression approach[35,36] to control for signal contribution from
212 draining veins. In particular, intra-cortical veins running perpendicular to the cortical surface are
213 known to drain blood from deeper layers of the cortex to larger pial veins situated along the grey
214 matter surface, resulting in loss of spatial specificity and intra-layer BOLD signal contamination.
215 To unmix the signal from adjacent layers, for each voxel in the superficial layers, we found the
216 nearest neighbor in the middle layer. We regressed out the mean time course of these voxels
217 assigned to middle layers from the time course of voxels assigned to superficial layers. MVPA
218 analysis following this correction showed a significant interaction between orientation and
219 session ($F(1,12) = 14.357$, $p = 0.003$, Figure S2A), consistent with learning-dependent changes
220 in superficial layers. Further, we observed enhanced discriminability in superficial layers after
221 correction for the trained orientation ($t(12) = -2.292$, $p = 0.041$), but not the untrained orientation
222 ($t(12) = 0.246$, $p = 0.810$). Learning-dependent changes in superficial V1 layers remained
223 significant after these corrections, suggesting that our results are unlikely to be significantly
224 confounded by vasculature-related artifacts.

Third, comparing mean normalized fMRI responses (Figure S3) across orientations and sessions did not show any significant results (three-way interaction (orientation × session × layer): $F(4,48) = 1.259$, $p = 0.299$, two-way interaction (orientation × session) in the superficial layers: $F(2,24) = 0.814$, $p = 0.455$, middle layers: $F(2,24) = 0.934$, $p = 0.407$ and deeper layers: $F(2,24) = 0.389$, $p = 0.682$), suggesting that the learning-dependent effects we observed reflect changes in orientation-specific representations across voxel patterns rather than mean univariate fMRI responses.

Fourth, we corroborated our results using a correlation-based pattern analysis[37] that showed learning-dependent changes in superficial V1 layers for the trained compared to the untrained orientation (Figure S2B). Specifically, Fisher z comparisons showed a significant orientation × session interaction in superficial V1 layers ($F(1,12) = 6.069$, $p = 0.030$), but not in middle ($F(1,12) = 2.382$, $p = 0.149$) nor deeper layers ($F(1,12) = 1.227$, $p = 0.290$).

Taken together, these results demonstrate enhanced orientation-specific representations in superficial rather than middle or deeper V1 layers after training, suggesting that learning alters read-out rather than input processing in V1. Similar learning-dependent effects with stronger learning-dependent changes in superficial layers were observed across visual areas (V1, V2, V3, V4, Figure S4). In particular, a repeated measures ANOVA showed no significant ROI x orientation x session x layer interaction ($F(2,24) = 1.459$, $p = 0.252$), but a significant orientation x session x layer interaction ($F(2,24) = 5.305$, $p = 0.012$), suggesting similar orientation-specific learning effects in superficial layers across visual areas.

Learning-dependent changes independent of task-context in the visual cortex

Our results showed learning-dependent changes in orientation-specific representations when participants performed a fine orientation discrimination task. To test whether the task performed by the participants is critical for this orientation-specific plasticity, we tested a subset of participants (n = 8) in a second post-training fMRI session while performing a control task (i.e. contrast change detection task) on identical stimuli to those presented to the participants during the post-training fMRI session. Before this additional scanning session, we conducted behavioral tests to ensure that perceptual improvement was retained. We observed that threshold performance (Mean = 1.78°, SD = 0.43°) did not differ significantly from the mean threshold of training day 5 (Mean = 1.69°, SD = 0.37°, paired t-test, $t(7) = -1.553$, $p = 0.164$). Further, we matched task difficulty in the contrast change detection task (~79.4%) to performance in the orientation discrimination task during the post-training fMRI session to ensure that the two post-training scanning sessions did not differ in task difficulty.

MVPA analysis across cortical layers in V1 showed that the learning-dependent changes we observed in orientation-specific representations in superficial layers were maintained when participants performed the control task. In particular, a two-way repeated measures ANOVA (orientation × task) on the MVPA accuracy showed a significant main effect of orientation ($F(1,7) = 19.140$, $p = 0.003$) in superficial V1 layers (Figure 5B). Neither the main effect of task ($F(1,7) = 2.608$, $p = 0.150$) nor the interaction effect ($F(1,7) = 0.082$, $p = 0.783$) were significant. We did not find any significant main or interaction effects in the deeper or middle layers of V1 (all $ps > 0.071$). These results suggest that learning-dependent changes in orientation-specific representations in superficial V1 layers are independent of task context, consistent with previous

neurophysiology results[9] showing learning-dependent changes in neural tuning in primary visual cortex during a fixation task.

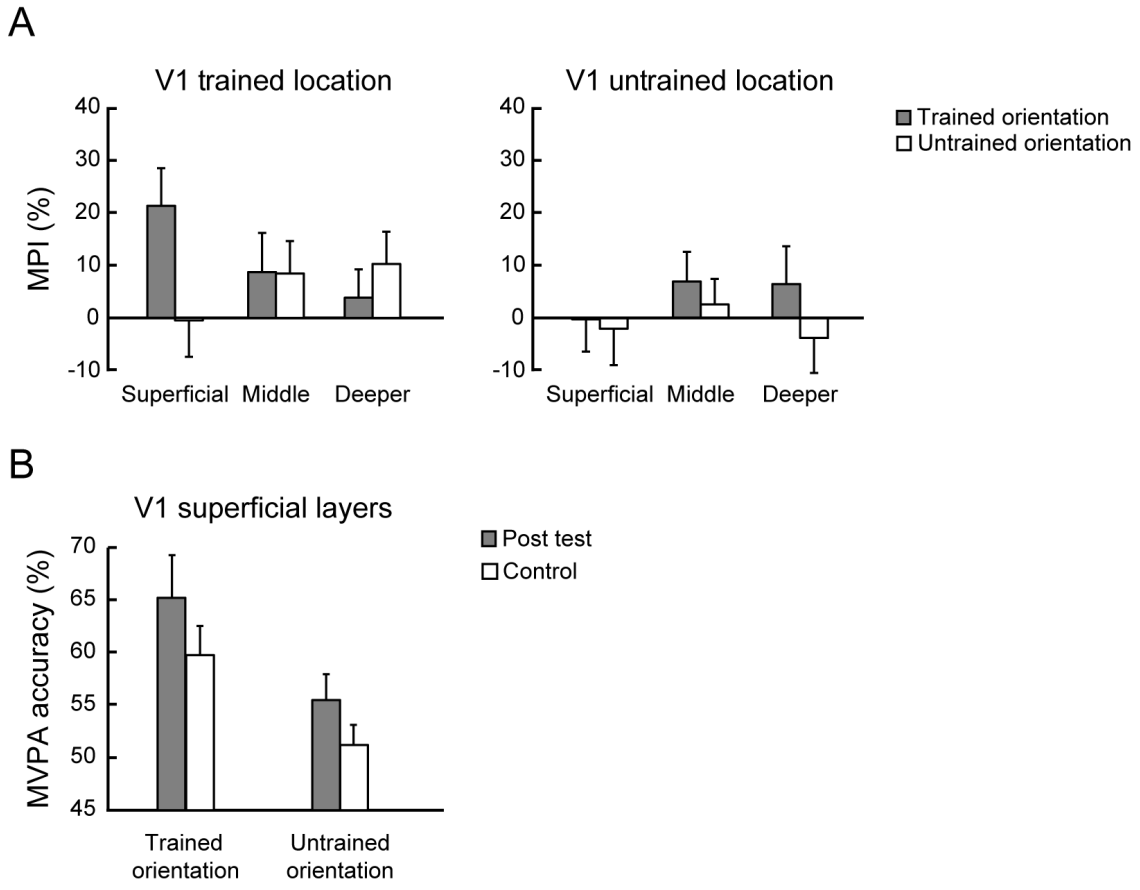

Figure 5. Learning-dependent changes in V1.

(A) Mean improvement index (MPI: (post-test accuracy – pre-test accuracy) / pre-test accuracy × 100%) for the trained and untrained orientations across V1 layers. The left panel shows significantly higher MPI for the trained than the untrained orientation at the trained location in superficial V1 layers, as indicated by significantly higher MPI for the trained than untrained orientation in the superficial layers ($t(12) = 3.218$, $p = 0.007$). The right panel shows no significant differences in MPI across layers for orientations presented at the untrained location. In particular, there was no significant differences in MPI for trained vs. untrained orientations in the superficial layers ($t(12) = 0.396$, $p = 0.699$). (B) MVPA accuracy for the

trained and untrained orientation at the trained location after training (post-test) compared to the control experiment in superficial layers of V1. Error bars indicate standard error of the mean across participants.

Learning-dependent changes in intraparietal cortex

We next considered learning-dependent changes in decision-making related areas[6,38] outside the visual cortex. In particular, we focused on IPS1 and IPS2 that have been implicated in perceptual decision making[38]. Using MVPA, we tested for learning-dependent changes in orientation representations across cortical depth. Figure 6 shows learning-dependent changes for the trained compared to the untrained orientation (i.e. increased MVPA accuracy for the trained orientation in the trained location) in middle rather than superficial or deeper layers. In particular, we observed a significant orientation × session interaction in middle layers of IPS ($F(1,12) = 6.324$, $p = 0.027$), but not in superficial ($F(1,12) = 0.502$, $p = 0.492$), nor deeper ($F(1,12) = 2.452$, $p = 0.143$) layers. Further, we observed significantly increased MVPA accuracy after training for the trained orientation in the middle ($t(12) = -3.432$, $p = 0.005$), but not superficial ($t(12) = 0.392$, $p = 0.702$), nor deeper ($t(12) = -1.137$, $p = 0.278$) layers, suggesting enhanced discriminability for the trained orientation in middle layers. In contrast, we did not observe any significant learning-dependent changes for the untrained location. In particular, there was no significant orientation × session interactions across IPS layers (superficial layers: $F(1,12) = 0.136$, $p = 0.718$; middle layers: $F(1,12) = 1.053$, $p = 0.325$; deeper layers: $F(1,12) = 1.628$, $p = 0.226$). Comparing learning-dependent changes in visual and posterior parietal cortex showed dissociable results. That is, we observed learning-dependent changes in superficial layers of visual cortex, while middle layers of posterior parietal cortex, as indicated by a significant ROI (V1, IPS) x session x layer interaction for the trained orientation (repeated measures ANOVA, $F(2,24) = 5.872$, $p =$

0.008), but not the untrained orientation (repeated measures ANOVA, F(2,24) = 1.933, p = 0.167).

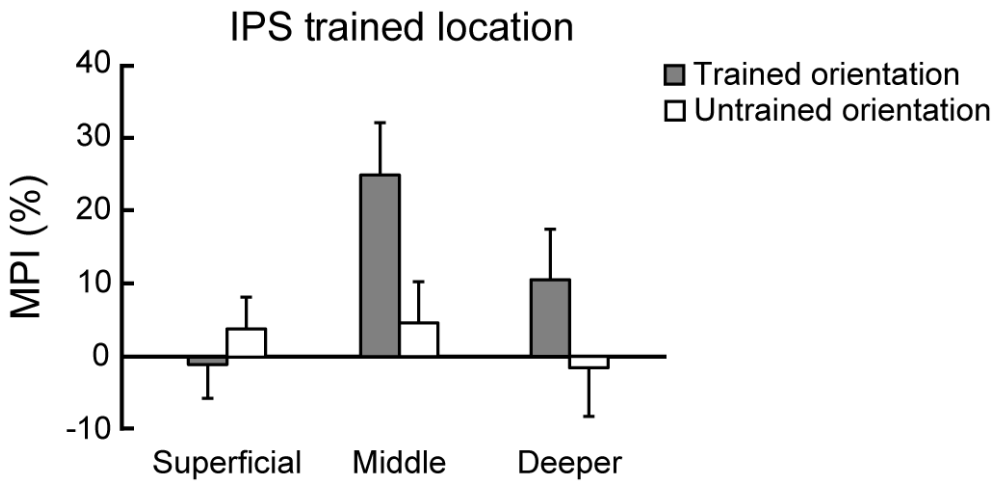

Figure 6. Learning-dependent changes in IPS.

Mean improvement index across IPS layers for the trained and untrained orientations presented at the trained location. The results showed significantly higher MPI for the trained than the untrained orientation at the trained location in the middle IPS layers (t(12) = 2.861, p = 0.014), but not in superficial (t(12) = -0.695, p = 0.500), nor deeper (t(12) = 1.382, p = 0.192) layers. Error bars indicate standard error of the mean across participants.

Informational connectivity analysis

Our results so far showed learning-dependent changes in orientation-specific representations in the superficial layers of V1 and middle layers of IPS, suggesting that learning modifies read-out rather than input signals in visual cortex, while input signals in posterior parietal cortex. Based on these results, we asked whether learning enhances functional connectivity between visual and posterior parietal cortex. To test this hypothesis, we employed an informational connectivity analysis[36] and tested whether V1 and IPS shared synchronous discriminability of multi-voxel

323 patterns that changed with training. Consistent with previous studies[19,20,26], we contrasted two
324 possible functional connectivity mechanisms: a) feedforward learning, as indicated by changes in
325 connectivity between superficial V1 layers and middle IPS layers, b) feedback learning, as
326 indicated by changes in connectivity between V1 deeper layers and IPS deeper layers. We did
327 not test functional connectivity between V1 superficial layers and deeper layers of higher areas,
328 as it is known to relate to both feedback and feedforward processing (Figure 1).

329 Following previous studies employing an informational connectivity analysis[36], we
330 interrogated the MVPA classifiers and extracted the distance from the hyperplane for the mean
331 pattern signal per block. For each layer per ROI we generated a time course of distance values
332 across blocks, regressed out the distance from other layers within the ROI and calculated the
333 partial Spearman correlation between V1 and IPS layers across blocks (Figure 7A). Our results
334 showed enhanced feedforward compared to feedback connectivity between V1 and IPS after
335 training. A repeated measures ANOVA (Fisher's z) showed a significant pathway (feedforward,
336 feedback) x orientation (trained vs. untrained) x session (pre-test, post-test) interaction ($F(1,12) =$
337 8.912, $p = 0.011$, Figure 7B).

338 In particular, we observed enhanced feedforward connectivity between superficial V1 layers
339 and middle IPS layers after training. A repeated measures ANOVA (Fisher's z) showed a
340 significant orientation × session interaction ($F(1,12) = 5.771$, $p = 0.033$), but no significant main
341 effect of orientation ($F(1,12) = 1.218$, $p = 0.291$) nor session ($F(1,12) = 2.326$, $p = 0.153$). Post-
342 hoc comparisons showed enhanced connectivity for the trained orientation ($t(12) = -2.599$, $p =$
343 0.023), but not the untrained orientation ($t(12) = 1.560$, $p = 0.145$). In contrast, we did not
344 observe any significant learning-dependent changes in feedback connectivity between deeper V1
345 and deeper IPS layers (orientation × session interaction: $F(1,12) = 0.587$, $p = 0.458$, main effect

346 of session: F(1,12) = 0.299, p = 0.595, main effect of orientation: F(1,12) = 1.223, p = 0.290).
347 This enhanced connectivity between superficial layers of V1 and middle layers of IPS after
348 training suggests that training alters feedforward information processing from sensory to
349 decision-related areas to support learning-dependent improvement in the fine orientation
350 discrimination task.
351

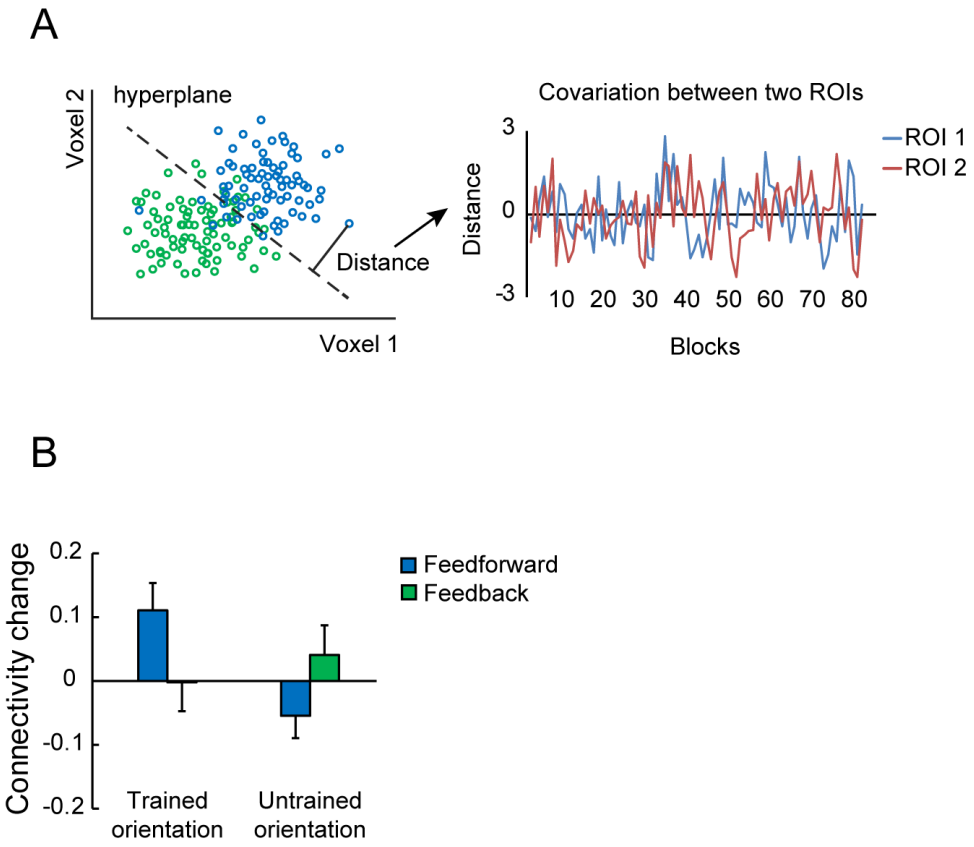

352

353 **Figure 7. Informational connectivity analysis.**
354 (A) Schematic illustration of the procedure followed for the MVPA-based functional connectivity
355 analysis. For each ROI and block, the distance to the hyperplane was used as an index of pattern
356 discriminability (left panel). Spearman correlation was used to calculate covariance between two ROIs
357 (right panel). (B) Learning-dependent changes (Fisher's z post- minus pre-test) in functional connectivity
358 between superficial V1 layers and middle IPS layers (feedforward connectivity) and between deeper V1

359 and IPS layers (feedback connectivity) for the trained and untrained orientations. Error bars indicate
360 standard error of the mean across participants.
361
362 **Discussion**
363 Despite the key role of learning in optimizing perceptual decisions, an ability known as
364 perceptual learning, we lack a mechanistic account of how training molds the adult human brain.
365 Evidence on experience-dependent plasticity mechanisms remains controversial with some
366 studies suggesting that learning modifies sensory encoding, while others proposing top-down
367 influences via feedback[5,39,40]. Conventional brain imaging techniques have been unable to
368 differentiate these possibilities due to limited spatial resolution[18]. Here, we capitalize on the sub-
369 millimeter resolution of 7T laminar fMRI to interrogate plasticity mechanisms across cortical
370 depths that are known to be associated with dissociable neural computations. Our results provide
371 evidence for recurrent experience-dependent plasticity mechanisms, offering an alternate
372 proposal for the neural instantiation of perceptual learning, by contrast to the long-standing
373 debate on encoding vs. feedback mechanisms of sensory plasticity.
374 Combining 7T laminar fMRI with MVPA we demonstrate enhanced decoding of
375 orientation-specific representations in superficial rather than middle layers of V1, suggesting that
376 learning modifies read-out rather than input signals in visual cortex[26]. Previous fMRI studies
377 using multi-voxel pattern classification approaches have shown that learning fine feature
378 discriminations increases the discriminability of neural representations[12,41]. Other brain imaging
379 studies[11,13,42,43] have shown learning-dependent changes in overall BOLD signal in V1. These
380 fMRI results have been interpreted broadly in support of an early neural locus of perceptual
381 learning. However, we still lack a mechanistic account of experience-dependent plasticity in the
382 human brain, as fMRI at standard resolution does not allow us to discern encoding from read-out

383 processes. Our layer-specific fMRI results propose that learning alters the processing of read-out
384 signals in superficial V1 layers rather than stimulus encoding in middle layers. It is unlikely that
385 this learning-dependent plasticity in superficial layers relates to stronger orientation selectivity in
386 superficial V1 layers, as recent quantitative measurements show nearly uniform distribution of
387 orientation selectivity across V1 layers than reported in early physiological studies[44]. Further, we
388 found that MVPA accuracy did not differ significantly across layers before training, suggesting
389 that learning-dependent changes in superficial V1 layers could not be due to differences in
390 orientation selectivity across V1 layers.

391 A possible explanation is that learning-dependent changes in superficial layers reflect top-
392 down influences via feedback[45,46]. It is possible that neurons with cell bodies in deeper layers and
393 dendrites projecting to the superficial layers result in learning-dependent changes in BOLD
394 signals in superficial layers[20,21]. However, this interpretation is less likely for three main reasons.
395 First, we did not observe learning-dependent changes in deeper V1 layers that are known to
396 receive long-range feedback. Second, our functional connectivity analysis showed enhanced
397 feedforward rather than feedback connectivity in occipito-parietal circuits. Third, consistent with
398 a previous physiological study[9], learning-dependent changes in superficial V1 layers were
399 maintained independent of task context; that is, these changes were evident not only when
400 participants performed the orientation discrimination task, but also when they performed a
401 contrast detection task (i.e. control experiment) that does not involve task-related feedback on
402 the trained stimulus dimension (i.e. orientation). It is possible that top-down influences, via
403 feedback connections to superficial layers, play a role in shaping visual feature templates at
404 earlier than later stages of training on the discrimination task[47]. However, interrogating the

405 representations of trained features after training reveals learning-dependent changes in
406 superficial layers that are independent of task context.

407 An alternate proposal is that orientation-specific learning-dependent changes in superficial
408 V1 layers are due to recurrent processing related to iso-orientation inhibition[48]; that is,
409 suppression of neurons that are selective for the same orientation across columns. Iso-orientation
410 inhibition is shown to be more pronounced in superficial layers and support orientation tuning
411 via horizontal connections between V1 columns[19,23,24]. It is possible that iso-orientation
412 suppression supports enhanced neural tuning to the trained orientation in superficial V1 layers,
413 suggesting a recurrent experience-dependent plasticity mechanism that alters orientation-specific
414 representations within visual cortex. These results are consistent with computational models
415 proposing that training sharpens neural tuning by altering recurrent connections (i.e. reducing
416 excitatory or increasing inhibitory connections) near the trained orientation[25,49] and
417 neurophysiological studies showing changes in orientation tuning due to training in visual cortex
418 [9,10]. Further horizontal connections in superficial V1 layers have been suggested to support
419 recurrent processing in the context of figure-ground segmentation[26] and experience-dependent
420 plasticity in the context of contour integration[2]. In particular, boundary detection was evidenced
421 in superficial layers ~30 ms after the initial visual response in the middle layers[26]. Future studies
422 combining laminar fMRI with EEG in humans have the potential to test whether learning-
423 dependent changes in superficial layers follow early sensory processing in middle layers,
424 revealing the dynamics of recurrent experience-dependent plasticity[26,27].

425 It is important to note that despite the advances afforded by laminar fMRI, GE-EPI is
426 limited by vasculature contribution to BOLD signals at the cortical surface resulting in loss of
427 spatial specificity[33]. Here, we demonstrate layer-specific learning-dependent changes following

428 several control analyses for these potential confounds, suggesting that our results are unlikely to
429 be confounded by vasculature-related artefacts. Our results are consistent with previous laminar
430 imaging studies showing BOLD effects in superficial layers in a range of tasks[28,29,45,46] and could
431 not be simply attributed to differences in attention due to task difficulty, as participant
432 performance was matched across sessions (pre vs. post-training). Future work could exploit
433 recent advances in CBV imaging using vascular space occupancy (VASO)[50] to enhance the
434 spatial specificity of laminar imaging in the human brain.

435 Extending beyond the visual cortex, we demonstrate learning-dependent changes in
436 posterior parietal cortex regions (IPS) that have been suggested to play a key role in perceptual
437 decision making[6]. In particular, we observed learning-dependent changes in fMRI activation
438 patterns in middle layers of IPS regions, suggesting that training alters input signals to posterior
439 parietal cortex. These results are consistent with previous neurophysiological[6] and human brain
440 imaging studies[38] that show learning-dependent changes in intraparietal cortex for perceptual
441 decision-making. Our findings provide new insights in understanding the finer scale circuit that
442 mediates experience-dependent plasticity across human brain systems, involving both sensory
443 and decision-related areas[51].

444 Further, we interrogated learning-dependent changes in functional connectivity[38,52]. We
445 tested whether training alters the functional connectivity within this circuit at the finer scale of
446 layer-to-layer interactions. Computational approaches have proposed that training strengthens the
447 connections between the most informative neurons in sensory areas and decision-related areas
448 via Hebbian learning, resulting in re-weighting of sensory signals in visual cortex[5]. In contrast,
449 the reverse hierarchy theory proposes that learning is implemented by top-down influences to
450 visual processing via long-range feedback from downstream areas[17]. To test these hypotheses,

451 we interrogated the layer-to-layer functional connectivity between visual and posterior parietal
452 cortex that allows us to compare feedforward vs. feedback processing based on known
453 anatomical connectivity models[19,20,53]. We demonstrate that learning strengthens feedforward
454 connectivity between superficial V1 layers and middle layers of IPS, consistent with previous
455 studies showing that ascending projections of V1 originate predominantly from the superficial
456 layers and ascending projections to IPS mainly terminate in middle layers[19,20,26]. In contrast, we
457 did not find any significant changes in feedback connectivity between deeper V1 and deeper IPS
458 layers, consistent with the lack of significant learning-dependent changes in deeper V1 layers.
459 Taken together, these results suggest that learning fine feature differences is implemented by re-
460 weighting mechanisms of visual plasticity rather than long-range feedback from decision-related
461 to visual areas. Corroborating evidence comes from the results of our control experiment
462 showing that learning-dependent changes in superficial V1 layers were maintained when
463 observers performed a contrast change detection task that does not involve orientation judgments
464 and therefore does not engage decision-related feedback on the trained stimulus dimension.

465 In sum, combining ultra-high field 7T imaging with a classic perceptual learning paradigm,
466 we provide evidence for recurrent mechanisms of experience-dependent plasticity that gate
467 perceptual decision making in the adult human brain. These mechanisms support re-weighting of
468 input signals in the visual cortex that are read-out by posterior parietal cortex to inform improved
469 perceptual decisions due to training. Interrogating experience-dependent plasticity at the finer
470 resolution afforded by UHF imaging using training paradigms that have been extensively tested
471 in both animals and humans, we provide the first insights in bridging the gap between animal
472 studies of micro-circuit plasticity and human fMRI studies of macro-scale network re-
473 organization. Understanding the mechanisms of experience-dependent plasticity in the adult

474 brain across scales and species is critical for designing effective training interventions that
475 support lifelong learning and adaptive behavior.
476

Materials and Methods

Participants

Fifteen participants (7 females; mean age: 27.87 years and SD: 3.83 years) took part in this study. Data from two participants were excluded from further analysis due to excessive head movement (See MRI data analysis) and technical issues during acquisition. As there are no previous UHF imaging studies on perceptual learning, we determined the sample size based on a previous 3T fMRI study on perceptual learning using an orientation discrimination task (N = 12)[12]. All participants had normal or corrected-to-normal vision, and were right-handed. Participants were naïve to the aim of the study, gave written informed consent and received payment for their participation. The study was approved by the University of Cambridge Ethics committee.

Stimuli and Apparatus

Stimuli comprised oriented sinusoidal gratings that were presented at an eccentricity of 5°, in the left or the right visual field against a uniform gray background. Gratings of random phase had a fixed diameter of 6°, contrast of 0.8, spatial frequency of 1 cycle/degree. The contrast decreased to zero over the outer 0.5° radius of the gratings.

Experiments were controlled using MATLAB and Psychophysics toolbox 3.0[54,55]. For the behavioral sessions, stimuli were presented on a 21-inch CRT monitor (1600 × 1200 pixel resolution, 85 Hz frame rate) at a distance of 110 cm. Gamma correction was applied to the monitor. For the fMRI scans, stimuli were presented using a projector and a mirror setup (1920 × 1080 pixel resolution, 100 Hz frame rate) at a viewing distance of 110 cm. Angular stimulus size was the same across behavioral and fMRI sessions.

500 **Experimental design**

501 The study comprised a pre-test (2 sessions, 1 behavioral test, 1 fMRI test), a training (5 sessions),
502 a post-test (2 sessions, 1 behavioral test, 1 fMRI test) and a control (2 sessions: 1 training, 1
503 fMRI test) phase (Figure 2A). All training and post-test sessions were conducted on consecutive
504 days.

505 We employed a two-interval forced choice (2IFC) orientation discrimination task (Figure
506 2B). Each trial began with a fixation cross for 200 ms followed by the sample and test gratings
507 that were presented sequentially for 200 ms each and separated by a 600 ms inter-stimulus
508 interval (ISI). Participants were asked to fixate and report (by key press) within 1270 ms after the
509 onset of the test grating whether it was tilted clockwise or counter-clockwise relative to the
510 sample stimulus.

511 Participants' performance in the task was measured using a 3-down-1-up staircase with 15
512 reversals converging at 79.4% performance. The reference orientation for the trained and
513 untrained stimuli was 55° or 125°. We added a uniformly distributed random jitter within ±5° to
514 the reference orientation across trials to ensure that participants compared two gratings in each
515 trial, rather than the test grating to a fixed reference orientation. The training reference
516 orientation (55° vs. 125°) was counterbalanced across participants. Participants were tested with
517 a control orientation (0°, vertical) that differed equally from the trained and untrained orientation
518 (55° or 125°). This allowed us to test orientation-specific pattern changes in fMRI signals due to
519 training (i.e. learning-dependent changes to the trained vs. untrained orientation), by comparing
520 separately the trained vs. the untrained orientations to the control orientation.

521 *Behavioral Tests.* To familiarize participants with the task before testing, each participant
522 performed a 30-trial practice run (5 trials per condition, i.e. three different reference orientations

523 at two different locations) using a fixed above-threshold angle difference (8°). For both the pre-
524 and post-training test, participants performed the orientation discrimination task for 12 test
525 staircase runs (2 runs per condition in random order). For each condition, the starting angle
526 difference between sample and test stimulus for the first run was 5°. For the second run, the
527 starting angle difference was determined by the threshold in the preceding run. The
528 discrimination threshold for each condition was the mean threshold across two runs. No feedback
529 was provided to the participants during the test phase.

530 *Behavioral Training (5 sessions).* We trained participants on the orientation discrimination task
531 (16 staircases per session, ~1 h) with gratings presented at the same orientation and location
532 throughout training. The starting angle difference between sample and test stimuli for the first
533 staircase of the first training session was 5°. For the remaining staircases, the starting angle
534 difference was determined by the threshold of the preceding staircase. Training location (i.e., left
535 vs. right visual field) and orientation (i.e., 55° vs. 125°) were counterbalanced across participants.
536 Participants were given auditory error feedback per trial.

537 *fMRI sessions.* Before and after training in the lab, participants completed 8-10 runs of the
538 orientation discrimination task during scanning. For each participant, we also collected data from
539 an anatomical scan and a retinotopic mapping scan.

540 For the orientation discrimination task, each run started with a fixation block (12.36 sec)
541 followed by one block for each of the six conditions and a fixation block. This sequence of
542 fixation and condition blocks was repeated four times in each run. Each condition block lasted
543 12.36 sec and comprised gratings presented at the trained, untrained or control orientation at one
544 of two locations (trained vs. untrained location). The order of orientations was randomized
545 across the six condition blocks and the stimulus location alternated between blocks. For each

546 block, participants completed five trials of the orientation discrimination task. The task
547 parameters (i.e. sample and test duration) were the same as for the behavioral tests and no
548 feedback was provided to the participants. The fixed angle difference between sample and test
549 stimuli for each condition was determined by the preceding behavioral session. This allowed us
550 to match task difficulty (~79.4%) before and after training.

551 *Control experiment*. To test the task specificity of the learning effect, eight participants
552 completed an additional training and fMRI session on consecutive days to ensure that learning
553 was maintained during a control task. The procedure for this control-task session was identical to
554 that for the post-training scan, with the exception that participants performed a contrast change
555 detection task. Participants were required to press a key within 1000 ms of detecting a contrast
556 change on the stimuli. The magnitude of contrast change was estimated for each participant
557 during the anatomical scan to ensure similar task difficulty (~79.4%) between the orientation
558 discrimination task and the contrast detection task. The estimated magnitude was fixed and used
559 throughout the control-task fMRI session.

560 **MRI data acquisition**

561 Imaging data were acquired at the Wolfson Brain Imaging Centre, University of Cambridge, on a
562 Siemens 7T Terra scanner with a 32-channel phased-array head coil (Nova Medical, Inc.,
563 Wilmington, MA, USA). For each participant, anatomical images were acquired using
564 MP2RAGE T1-weighted sequence (TR = 5000 ms, TE = 2.56 ms, FOV = 208 × 208 mm^2,
565 resolution 0.65 × 0.65 × 0.65 mm^3, number of slices: 240, slice orientation: sagittal). Functional
566 scans were acquired using a 2D Gradient Echo, Echo Planar Imaging (GE-EPI) sequence[56] (TR =
567 2060 ms, TE = 26.4 ms, FOV = 148 × 148 mm^2, flip angle: 70°, resolution 0.8 × 0.8 × 0.8 mm^3,
568 number of slices: 56, partial Fourier = 6/8, GRAPPA factor = 3, Multi-Band factor = 2,

569 bandwidth = 1034 Hz/Pixel, echo spacing = 1.09 ms). The field of view covered occipito-
570 temporal and posterior parietal areas; manual shimming was performed prior to the acquisition of
571 the functional scans.

572 **Behavioral data analysis**

573 Performance was measured by the 3-down-1-up staircase with 15 reversals. The mean angle
574 difference of the last 8 reversals was taken as the threshold of each staircase run. The measured
575 orientation discrimination thresholds were used as the dependent factor. Using a within-subject
576 factorial design, we manipulated three independent factors, the reference orientation (trained and
577 untrained orientation), stimulus location (trained and untrained location) and test session (pre-test,
578 post-test), to evaluate the learning effect and learning specificity. Further, we calculated the
579 mean percent improvement index (MPI, (pre-test threshold – post-test threshold) / pre-test
580 threshold × 100%)) for each condition. For statistical analysis, we used repeated measures
581 ANOVAs to compare across conditions.

582 **MRI data analysis**

583 *Anatomical data analyses.* T1-weighted anatomical data was used for coregistration and 3D
584 cortex reconstruction. Grey and white matter segmentation was obtained on the MP2RAGE
585 images using FreeSurfer (http://surfer.nmr.mgh.harvard.edu/) and manually improved for the
586 regions of interest (i.e., V1, V2, V3, V4, and IPS) using ITK-SNAP (www.itksnap.org). The
587 refined segmentation was used to obtain a measurement of cortical thickness. Following previous
588 studies, we assigned voxels to three layers (superficial, middle, deeper) using the equi-volume
589 approach[57,58] as implemented in BrainVoyager (Brain Innovation, Maastricht, The Netherlands).
590 This approach has been shown to reduce misclassification of voxels to layers, in particular for
591 regions of interest presenting high curvature. Information from the cortical thickness map and

592 gradient curvature was used to generate four grids at different cortical depths (ranging from 0:
593 white matter, to 1: grey matter). Mapping of each voxel to a layer was obtained by computing the
594 Euclidean distance of each grey matter voxel to the grids: the two closest grids represent the
595 borders of the layer to which a voxel is assigned (Figure 3B). The anatomical image was aligned
596 to the functional data using the boundary-based registration[59]. We assessed the alignment and
597 manually corrected if necessary.

598 *Functional data analyses.* The GE-EPI functional data were analysed using BrainVoyager
599 (version 20.6, Brain Innovation, Maastricht, The Netherlands) and custom MATLAB (The
600 MATHWORKS Inc., Natick, MA, USA) code. The first two volumes at the beginning of each
601 run were discarded to ensure that the longitudinal magnetization reached steady state. The
602 functional data were corrected for distortions due to non-zero off-resonance field (at the
603 beginning of each functional run, five volumes with inverted phase encoding direction were
604 acquired and used to estimate a voxel displacement map that was subsequently applied to the
605 functional data using COPE (Correction based on Opposite Phase Encoding, BrainVoyager,
606 Brain Innovation). The distortion-corrected data underwent slice-timing correction, head motion
607 correction (the single band image acquired at the beginning of the first run was used as the
608 reference in the alignment), high-pass temporal filtering (using a GLM with Fourier basis set at 2
609 cycles) and removal of linear trends. We then aligned the functional data across sessions. To
610 validate the alignment, we calculated the mean EPI image of each functional run for each region
611 of interest (ROI) and estimated the spatial correlation between these mean EPI images. We
612 performed manual adjustment of the alignment if the spatial correlation was below 0.85 and
613 excluded data from one participant for whom the alignment could not be improved manually.

614 *Regions of Interest definition.* We used the data from the retinotopic mapping scan to identify
615 visual areas based on standard phase-encoding methods. Participants viewed rotating wedges that
616 created travelling waves of neural activity[60,61]. Due to limited coverage during acquisition, area
617 V4 was identified for 8 of the 13 participants included in the analysis. Thus, for further analyses
618 we combined the data from V2, V3 and V4 for each individual participant. Further, we defined
619 regions in the intraparietal sulcus (IPS1, IPS2) given their functional relevance for perceptual
620 learning [6]. Intraparietal regions (IPS1 and IPS2) were defined for each participant based on
621 anatomical templates provided by Benson (https://hub.docker.com/r/nben/occipital_atlas/)[62].
622 This procedure uses the individual participant-based segmentation obtained with FreeSurfer and
623 an anatomical probabilistic template, to estimate the best location for the region of interest (i.e.
624 IPS). Each IPS subregion was subsequently inspected to ensure consistent definition across
625 participants.

626 For each of the visual cortex ROIs, we modelled BOLD signals using a GLM with two
627 regressors (i.e., left vs. right visual field) and included the estimated head motion parameters as
628 nuisance regressors. The resulting t-statistical map was thresholded ($t = 2.58$, $p = 0.01$) to select
629 voxels within each ROI that responded strongly to the lateralized stimulus presentation,
630 consistent with location specificity in visual cortex. For IPS, we selected voxels that responded
631 to the task irrespective of stimulus location (i.e. task vs. fixation, $t = 1.64$, $p = 0.10$).

632 *Correcting for vasculature-related effects:* Voxel selection within each ROI was further refined
633 by excluding voxels that were confounded by vasculature effects that are known to contribute to
634 a superficial bias in the measured BOLD signal; that is, increased BOLD with increasing
635 distance from white matter. In particular, it has been shown that the BOLD signal measured
636 using GE-EPI (i.e. T2* weighted) is confounded by macro- and micro-vasculature signals[32,63,64].

637 The macro-vasculature contribution is due to veins penetrating the grey matter and running
638 through its thickness, as well as large pial veins situated along the surface of the grey matter[65].
639 This results in increased sensitivity (i.e., strong BOLD effect) but decreased spatial specificity of
640 the measured signal. The latter can be understood by the mechanics of the draining veins
641 carrying deoxygenated haemoglobin downstream from the true neuronal site of neural activation,
642 leading to a response spatially biased towards the pial surface, an effect known as superficial bias.
643 Here, we took the following approach to reduce superficial bias due to vasculature
644 contributions. First, following previous work[66], we computed the temporal signal to noise ratio
645 (tSNR) for each voxel in each ROI (V1 V2, V3, V4 and IPS respectively). We used tSNR to
646 identify voxels near large veins that are expected to have large variance and low intensity signal
647 due to the local concentration of deoxygenated haemoglobin resulting in a short T2* decay time
648 (i.e., dark intensity in a T2* weighted image). We identified voxels with low tSNR, checked their
649 correspondence with voxels of lower intensities on the T2* weighted images. Second, it has been
650 shown that high t-values on a fMRI statistical map are likely to arise from large pial veins[67,68].
651 Therefore, voxels with low tSNR values or t-score values above the 90th percentile of the t-score
652 distribution obtained by the GLM described above were removed from further analysis. We used
653 these two approaches to correct the BOLD signal from confounding vasculature effects.
654 *Univariate analysis.* For each participant, test session, run and condition, we extracted the z-
655 scored fMRI responses between the 4th and 8th TR (i.e. 6.18 – 14.42 s) after block onset. This
656 time window captured the peak of the hemodynamic responses to the visual stimuli. The
657 normalized fMRI responses were averaged across time points, blocks and runs for each condition
658 and each session. Repeated-measures ANOVA was used to test the univariate difference across
659 conditions.

660 *Multivariate pattern analysis.* We used multivariate pattern analysis (MVPA) to decode: a)
661 trained vs. control orientation, b) untrained vs. control orientation. For each ROI and participant,
662 we calculated per voxel a t-score statistic by comparing activity for stimuli that were presented
663 left vs. right of the fixation (V1) or activity for task vs. fixation (IPS). We used this statistic to
664 rank the voxels within each ROI and selected voxels (500 for visual areas; 200 voxels for IPS)
665 with the higher t-score to include in the MVPA, as classification accuracy saturated across all
666 participants for these voxel pattern sizes in the corresponding regions (Figure S4). We used the
667 same number of voxels (i.e. 200 voxels) when comparing data between V1 and IPS and for the
668 informational connectivity analysis. This voxel selection procedure ensured that comparisons of
669 MVPA accuracy could not be confounded by varying number of voxels across participants. We
670 then extracted mean normalized fMRI responses between 4th to 8th TR (i.e. 6.18 – 14.42 s) after
671 block onset for this pattern of voxels per ROI, participant and test session. We trained a linear
672 classifier using LIBSVM (http://www.csie.ntu.edu.tw/~cjlin/libsvm/) implemented in MATLAB
673 to discriminate: a) the trained from the control orientation, b) the untrained from the control
674 orientation. As both the trained and untrained orientation differed equally from the control
675 orientation (~55°), we hypothesized that differences in the accuracy between these two
676 classification tasks would be due to training rather than stimulus differences. We computed
677 classification accuracy using a leave-one-run-out cross-validation. That is, we divided the data
678 set into training and test data with maximum 72 training patterns (for n = 7 participants with 8
679 runs) and 8 patterns for the test run. We averaged the classification accuracy across folds,
680 separately for each test session. We used repeated-measures ANOVAs to assess differences in
681 classification accuracy across conditions (orientation × session). Similar to the MPI for

682 behavioral data, we defined the MPI for decoding accuracy as (post-test accuracy – pre-test
683 accuracy) / pre-test accuracy × 100%).

684 Further, we performed a correlation-based pattern analysis[37] to consolidate our MVPA
685 results. In the correlation-based pattern analysis, the data and voxels used were identical to those
686 used in the MVPA analysis. We divided the data set into training and test data and performed a
687 leave-one-run-out cross-validation. For each dataset, we calculated the mean response of each
688 orientation for each voxel. We then calculated the Spearman correlation across voxels and
689 transformed the correlation coefficients using Fisher's z-transform. We hypothesized that the
690 correlation coefficient would be higher for data from the training and test set that related to the
691 same orientation (i.e. trained-trained orientation) than different orientations (i.e. trained-control
692 orientation). We used the difference between the same and different orientations to index the
693 information contained in each ROI. We used repeated-measures ANOVAs to examine
694 differences across conditions (orientation × session).

695 *Informational Connectivity analysis.* We used Informational Connectivity (IC) to identify layers
696 that share synchronized discriminability of activity related to stimulus-specific multi-voxel
697 pattern information[36,69,70]. We examined intercortical IC based on shared changes (fluctuations)
698 in pattern discriminability over time, as this approach has been shown to be more sensitive than
699 univariate functional connectivity. To track the flow of multivariate information across time (i.e.
700 across blocks), we measured the fluctuations (covariance) in MVPA discriminability by
701 calculating distance information from the classification hyperplane (Figure 7A). In particular, we
702 selected 200 voxels with the higher t-score and used the same multivoxel training vs. test
703 patterns as in the MVPA analysis. For each ROI and layer, we extracted distance information for
704 the test data per block from the trained classifiers. We calculated layer-specific connectivity by

705 partial Spearman correlation between the fold-wise distance of different layers; that is, for a
706 given layer, we regressed out the distance information from other layers within each ROI. We
707 transformed the correlation coefficients using Fisher's z-transform and conducted repeated
708 measures ANOVA to compare across conditions.

References

1. Gilbert, C. D., Sigman, M. & Crist, R. E. The Neural Basis of Perceptual Learning. *Neuron* **31**, 681–697 (2001).
2. Gilbert, C. D. & Li, W. Adult Visual Cortical Plasticity. *Neuron* **75**, 250–264 (2012).
3. Hooks, B. M. & Chen, C. Circuitry Underlying Experience-Dependent Plasticity in the Mouse Visual System. *Neuron* **106**, 21–36 (2020).
4. Sagi, D. & Tanne, D. Perceptual learning: learning to see. *Curr. Opin. Neurobiol.* **4**, 195–199 (1994).
5. Dosher, B. & Lu, Z.-L. Visual Perceptual Learning and Models. *Annu. Rev. Vis. Sci.* **3**, 343–363 (2017).
6. Law, C. T. & Gold, J. I. Shared mechanisms of perceptual learning and decision making. *Top. Cogn. Sci.* **2**, 226–238 (2010).
7. Ahissar, M. & Hochstein, S. Task difficulty and the specificity of perceptual learning. *Nature* **387**, 401–406 (1997).
8. Schoups, A. A., Vogels, R. & Orban, G. a. Human perceptual learning in identifying the oblique orientation: retinotopy, orientation specificity and monocularity. *J. Physiol.* **483**, 797–810 (1995).
9. Schoups, A., Vogels, R., Qian, N. & Orban, G. Practising orientation identification improves orientation coding in V1 neurons. *Nature* **412**, 549–553 (2001).
10. Yan, Y. *et al.* Perceptual training continuously refines neuronal population codes in primary visual cortex. *Nat. Neurosci.* **17**, 1380–1389 (2014).
11. Bao, M., Yang, L., Rios, C., He, B. & Engel, S. a. Perceptual Learning Increases the Strength of the Earliest Signals in Visual Cortex. *J. Neurosci.* **30**, 15080–15084 (2010).
12. Jehee, J. F. M., Ling, S., Swisher, J. D., Bergen, R. S. Van & Tong, F. Perceptual learning selectively refines orientation representations in Early Visual Cortex. *J. Neurosci.* **32**, 16747–16753 (2012).
13. Schwartz, S., Maquet, P. & Frith, C. Neural correlates of perceptual learning : A functional MRI study of visual texture discrimination. *Proc. Natl. Acad. Sci.* **99**, 17137–17142 (2002).
14. Raiguel, S., Vogels, R., Mysore, S. G. & Orban, G. a. Learning to see the difference specifically alters the most informative V4 neurons. *J. Neurosci.* **26**, 6589–6602 (2006).
15. Yang, T. & Maunsell, J. H. R. The Effect of Perceptual Learning on Neuronal Responses in Monkey Visual Area V4. *J. Neurosci.* **24**, 1617–1626 (2004).
16. Kahnt, T., Grueschow, M., Speck, O. & Haynes, J. D. Perceptual Learning and Decision-Making in Human Medial Frontal Cortex. *Neuron* **70**, 549–559 (2011).
17. Ahissar, M. & Hochstein, S. The reverse hierarchy theory of visual perceptual learning. *Trends Cogn. Sci.* **8**, 457–464 (2004).
18. Goense, J., Bohraus, Y. & Logothetis, N. K. fMRI at high spatial resolution: implications for BOLD-models. *Front. Comput. Neurosci.* **10**, (2016).
19. RockLand, K. S. & Pandya, D. N. Laminar origins and terminations of cortical connections of the occipital lobe in the rhesus monkey. *Brain Res.* **179**, 3–20 (1979).
20. Markov, N. T. *et al.* Anatomy of Hierarchy: Feedforward and Feedback Pathways in Macaque Visual Cortex. *J. Comp. Neurol.* **522**, 225–259 (2014).
21. Larkum, M. E., Petro, L. S., Sachdev, R. N. S. & Muckli, L. A Perspective on Cortical Layering and Layer-Spanning Neuronal Elements. *Front. Neuroanat.* **12**, (2018).

22. Self, M. W., van Kerkoerle, T., Goebel, R. & Roelfsema, P. R. Benchmarking laminar fMRI: Neuronal spiking and synaptic activity during top-down and bottom-up processing in the different layers of cortex. *Neuroimage* **197**, 806–817 (2019).
23. Gilbert, C. D. & Wiesel, T. Clustered intrinsic connections in cat visual cortex. *J. Neurosci.* **3**, 1116–1133 (1983).
24. Douglas, R. J. & Martin, K. A. C. Recurrent neuronal circuits in the neocortex. *Curr. Biol.* **17**, 496–500 (2007).
25. Schwabe, L. & Obermayer, K. Adaptivity of tuning functions in a generic recurrent network model of a cortical hypercolumn. *J. Neurosci.* **25**, 3323–3332 (2005).
26. Self, M. W., van Kerkoerle, T., Supèr, H. & Roelfsema, P. R. Distinct roles of the cortical layers of area V1 in figure-ground segregation. *Curr. Biol.* **23**, 2121–2129 (2013).
27. Buffalo, E. A., Fries, P., Landman, R., Buschman, T. J. & Desimone, R. Laminar differences in gamma and alpha coherence in the ventral stream. *Proc. Natl. Acad. Sci.* **108**, 11262–11267 (2011).
28. Martino, F. De *et al.* Frequency preference and attention effects across cortical depths in the human primary auditory cortex. *Proc. Natl. Acad. Sci.* **112**, 16036–16041 (2015).
29. Lawrence, S. J. D., Norris, D. G. & De Lange, F. P. Dissociable laminar profiles of concurrent bottom-up and top-down modulation in the human visual cortex. *Elife* **8**, 1–17 (2019).
30. Hung, S. & Seitz, A. R. Prolonged Training at Threshold Promotes Robust Retinotopic Specificity in Perceptual Learning. *J. Neurosci.* **34**, 8423–8431 (2014).
31. Zhang, J. Y. *et al.* Rule-based learning explains visual perceptual learning and its specificity and transfer. *J. Neurosci.* **30**, 12323–12328 (2010).
32. Uğurbil, K., Toth, L. & Kim, D. S. How accurate is magnetic resonance imaging of brain function? *Trends Neurosci.* **26**, 108–114 (2003).
33. Kay, K. *et al.* A critical assessment of data quality and venous effects in sub-millimeter fMRI. *Neuroimage* **189**, 847–869 (2019).
34. Vizioli, L. *et al.* Multivoxel Pattern of Blood Oxygen Level Dependent Activity can be sensitive to stimulus specific fine scale responses. *bioRxiv* (2019).
35. Kok, P. *et al.* Selective Activation of the Deep Layers of the Human Primary Visual Cortex by Top-Down Feedback. *Curr. Biol.* **26**, 371–376 (2016).
36. Koster, R., Chadwick, M. J., Chen, Y. & Kumaran, D. Big-Loop Recurrence within the Hippocampal System Supports Integration of Information across Episodes. *Neuron* **99**, 1342–1354 (2018).
37. Haxby, J. V. *et al.* Distributed and overlapping representations of faces and objects in ventral temporal cortex. *Science (80-.).* **293**, 2425–2430 (2001).
38. Chen, N. *et al.* Sharpened cortical tuning and enhanced cortico-cortical communication contribute to the long-term neural mechanisms of visual motion perceptual learning. *Neuroimage* **115**, 17–29 (2015).
39. Byers, A. & Serences, J. T. Exploring the relationship between perceptual learning and top-down attentional control. *Vision Res.* **74**, 30–39 (2012).
40. Gilbert, C. D., Li, W. & Piech, V. Perceptual learning and adult cortical plasticity. *J. Physiol.* **587**, 2743–51 (2009).
41. Zhang, J., Meeson, A., Welchman, A. E. & Kourtzi, Z. Learning alters the tuning of functional magnetic resonance imaging patterns for visual forms. *J. Neurosci.* **30**, 14127–14133 (2010).

42. Furmanski, C. S., Schluppeck, D. & Engel, S. A. Learning Strengthens the Response of Primary Visual Cortex to Simple Patterns. *Curr. Biol.* **14**, 573–578 (2004).
43. Mukai, I. *et al.* Activations in visual and attention-related areas predict and correlate with the degree of perceptual learning. *J. Neurosci.* **27**, 11401–11411 (2007).
44. Ringach, D. L., Shapley, R. M. & Hawken, M. J. Orientation selectivity in macaque V1: diversity and laminar dependence. *J. Neurosci.* **22**, 5639–5651 (2002).
45. Gau, R., Bazin, P.-L., Trampel, R., Turner, R. & Noppeney, U. Resolving multisensory and attentional influences across cortical depth in sensory cortices. *Elife* **9**, (2020).
46. Muckli, L. *et al.* Contextual Feedback to Superficial Layers of V1. *Curr. Biol.* **25**, 2690–2695 (2015).
47. Chang, D. H. F., Mevorach, C., Kourtzi, Z. & Welchman, A. E. Training transfers the limits on perception from parietal to ventral cortex. *Curr. Biol.* **24**, 2445–2450 (2014).
48. Malach, R., Amir, Y., Harel, M. & Grinvald, A. Relationship between intrinsic connections and functional architecture revealed by optical imaging and in vivo targeted biocytin injections in primate striate cortex. *Proc. Natl Acad. Sci. USA* **90**, 10469–10473 (1993).
49. Teich, A. F. & Qian, N. Learning and adaptation in a recurrent model of V1 orientation selectivity. *J. Neurophysiol.* **89**, 2086–2100 (2003).
50. Huber, L., Uludağ, K. & Möller, H. E. Non-BOLD contrast for laminar fMRI in humans: CBF, CBV, and CMRO2. *Neuroimage* **197**, 742–760 (2019).
51. Watanabe, T. & Sasaki, Y. Perceptual Learning: Toward a Comprehensive Theory. *Annu. Rev. Psychol.* **66**, 1–25 (2015).
52. Lewis, C. M., Baldassarre, A., Committeri, G., Romani, G. L. & Corbetta, M. Learning sculpts the spontaneous activity of the resting human brain. *Proc. Natl. Acad. Sci.* **106**, 17558–17563 (2009).
53. Van Essen, D. C. & Felleman, D. J. Distributed Hierarchical Processing in the Primate Cerebral Cortex. *Cereb. Cortex* **1**, 1–47 (1991).
54. Pelli, D. G. The VideoToolbox software for visual psychophysics: transforming numbers into movies. *Spat. Vis.* **10**, 437–442 (1997).
55. Brainard, D. H. The Psychophysics Toolbox. *Spat. Vis.* **10**, 433–436 (1997).
56. Moeller, S. *et al.* Multiband multislice GE-EPI at 7 tesla, with 16-fold acceleration using partial parallel imaging with application to high spatial and temporal whole-brain FMRI. *Magn. Reson. Med.* **63**, 1144–1153 (2010).
57. Waehnert, M. D. *et al.* Anatomically motivated modeling of cortical laminae. *Neuroimage* **93**, 210–220 (2014).
58. Kemper, V. G., De Martino, F., Emmerling, T. C., Yacoub, E. & Goebel, R. High resolution data analysis strategies for mesoscale human functional MRI at 7 and 9.4 T. *Neuroimage* **164**, 48–58 (2018).
59. Greve, D. N. & Fischl, B. Accurate and robust brain image alignment using boundary-based registration. *Neuroimage* **48**, 63–72 (2009).
60. Engel, S. a, Wandell, B. a & Glover, G. G. Retintopic organization in human visual cortex and the spatial precision of functional MRI. *Cereb. Cortex* **7**, 181–192 (1997).
61. Sereno, M. I. *et al.* Borders of Multiple Visual Areas In Humans Revealed By Functional MRI. *Science (80-.).* **268**, 889–893 (1995).
62. Wang, L., Mruczek, R. E. B., Arcaro, M. J. & Kastner, S. Probabilistic maps of visual topography in human cortex. *Cereb. Cortex* **25**, 3911–3931 (2015).

63. Uludağ, K., Müller-Bierl, B. & Uğurbil, K. An integrative model for neuronal activity-induced signal changes for gradient and spin echo functional imaging. *Neuroimage* **48**, 150–165 (2009).
64. Yacoub, E., Van De Moortele, P. F., Shmuel, A. & Uğurbil, K. Signal and noise characteristics of Hahn SE and GE BOLD fMRI at 7 T in humans. *Neuroimage* **24**, 738–750 (2005).
65. Duvernoy, H. M., Delon, S. & Vannson, J. L. Cortical blood vessels of the human brain. *Brain Res. Bull.* **7**, 519–579 (1981).
66. Olman, C. A., Inati, S. & Heeger, D. J. The effect of large veins on spatial localization with GE BOLD at 3 T: Displacement, not blurring. *Neuroimage* **34**, 1126–1135 (2007).
67. Polimeni, J. R., Fischl, B., Greve, D. N. & Wald, L. L. Laminar analysis of 7 T BOLD using an imposed spatial activation pattern in human V1. *Neuroimage* **52**, 1334–1346 (2010).
68. Kashyap, S., Ivanov, D., Havlicek, M., Poser, B. A. & Uludağ, K. Impact of acquisition and analysis strategies on cortical depth-dependent fMRI. *Neuroimage* **168**, 332–344 (2018).
69. Coutanche, M. N. & Thompson-Schill, S. L. Using informational connectivity to measure the synchronous emergence of fMRI multi-voxel information across time. *J. Vis. Exp.* 1–7 (2014) doi:10.3791/51226.
70. Anzellotti, S. & Coutanche, M. N. Beyond Functional Connectivity: Investigating Networks of Multivariate Representations. *Trends Cogn. Sci.* **22**, 258–269 (2018).

Acknowledgements:

We would like to thank Valentyna Chernova and Cher Zhou for help with the analysis. We are grateful to Cong Yu and Sheng Li for their helpful comments and suggestions on this work. This work was supported by grants to Z.K. from the Biotechnology and Biological Sciences Research Council (H012508 and BB/P021255/1), the Wellcome Trust (205067/Z/16/Z) and European Union's Horizon 2020 research and innovation programme under the Marie Skłodowska Curie grant agreement No 840271. The 7T MRI was funded by the MRC (MR/M008983/1) and the NIHR Cambridge Biomedical Research Centre. C.T.R. is funded by the Wellcome Trust and the Royal Society (098436/Z/12/B).

Author contributions:

K.J. and Z.K. conceived the project and designed the experiments. V.K., C.R., C.T.R., G.W. and R.G. developed the GE EPI protocol used in the study. K.J. and E.Z. performed the experiments. K.J., E.Z, N.R.G., and A.N. developed the analysis pipeline and analyzed the data. K.J. and Z.K. wrote the manuscript.

Declaration of interests:

The authors declare no competing interests.

Supplementary Material

Figures

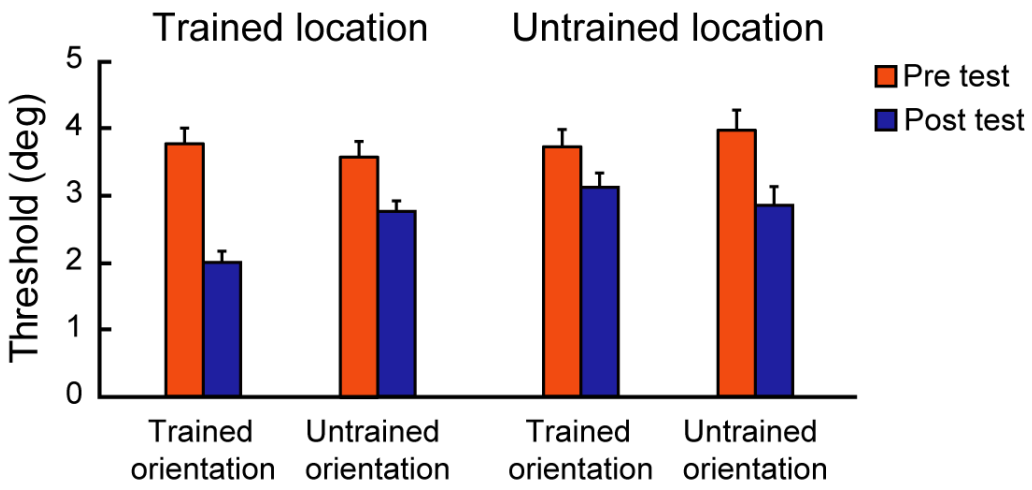

Figure S1. Behavioral results.

Mean performance across participants before and after training (pre-, post-test) at ~79.4% threshold for the trained and untrained orientations presented at the trained and untrained locations. Error bars indicate standard error of the mean across participants. We observed learning specificity for the trained orientation at the trained location, as indicated by a significant orientation × location × session interaction (repeated measures ANOVA, $F(1,12) = 11.858$, $p = 0.005$) and a significant orientation × session interaction ($F(1,12) = 21.551$, $p = 0.001$) at the trained, but not the untrained ($F(1,12) = 3.093$, $p = 0.104$) location. Post-hoc comparisons at the trained location showed significantly lower threshold for the trained than the untrained orientation after ($t(12) = -5.208$, $p < 0.001$), but not before ($t(12) = 1.264$, $p = 0.230$) training. In contrast, no significant differences between the trained and the untrained orientations were observed at the untrained location (pre-test session: $t(12) = -1.203$, $p = 0.252$, post-test session: $t(12) = 1.066$, $p = 0.308$).

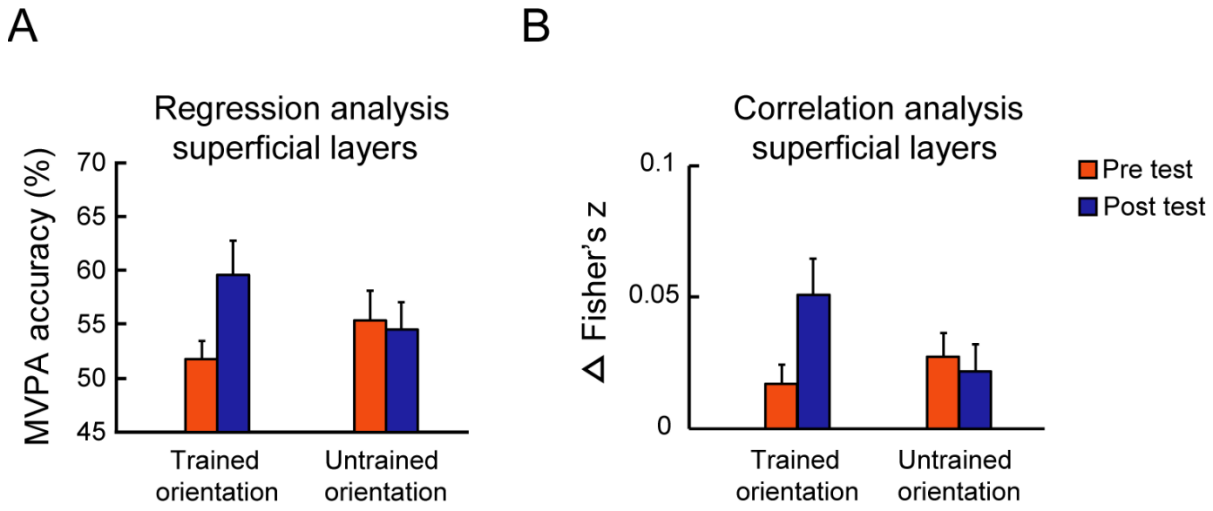

Figure S2. Control analyses.

(A) MVPA accuracy before and after training for the trained and untrained orientations presented at the trained location in superficial V1 layers after regressing out the signal from the adjacent voxels in middle layers. (B) Correlation-based pattern analysis. Correlation differences (correlation of mean normalized BOLD across voxels for the same orientation minus normalized BOLD for different orientations) for the trained and untrained orientations presented at the trained location in superficial V1 layers. Error bars indicate standard error of the mean across participants.

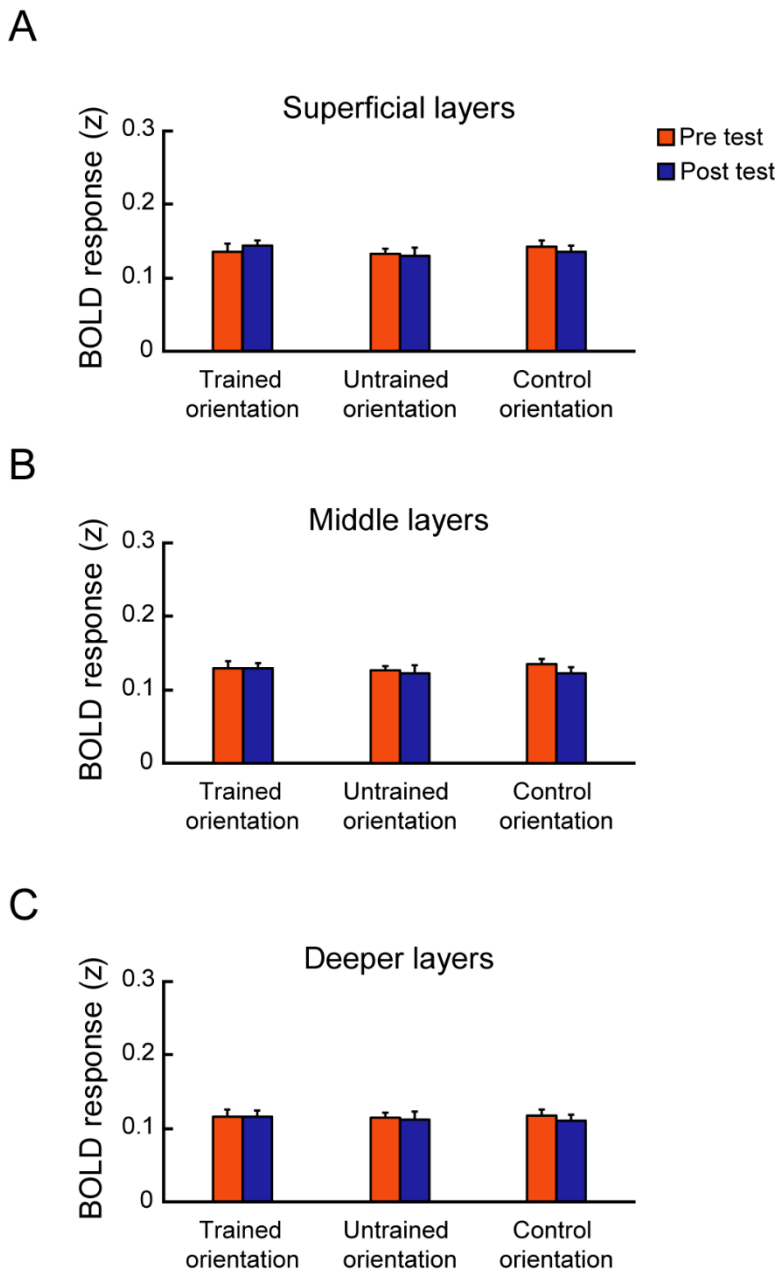

Figure S3. Univariate fMRI analysis.

Mean normalized BOLD before and after training for the trained, untrained and control orientations presented at the trained location across V1 layers. Error bars indicate standard error of the mean across participants.

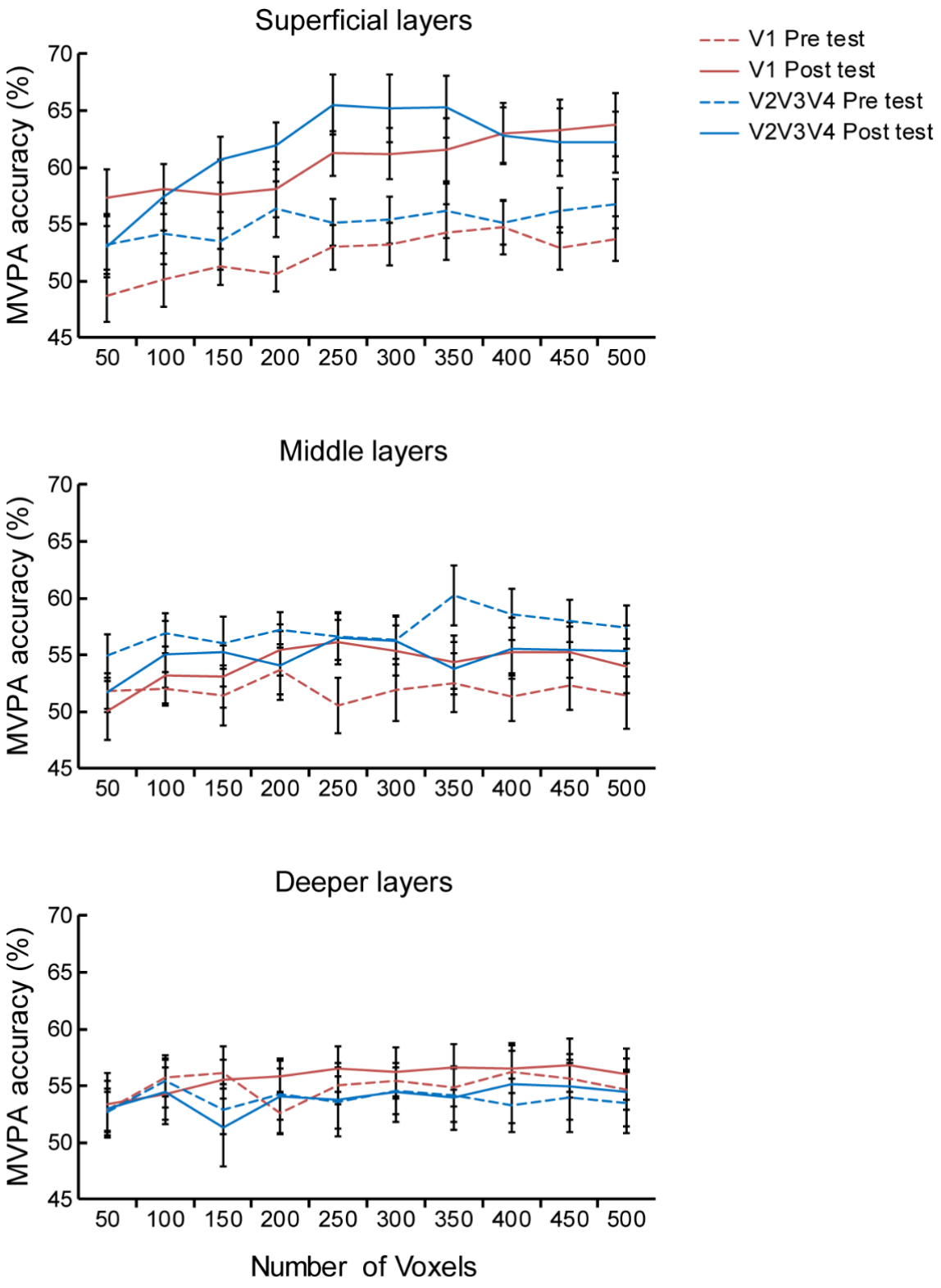
Superficial layers
Middle layers
Deeper layers
MVPA accuracy (%)
70
65
60
55
50
45
50
100
150
200
250
300
350
400
450
500
Number of Voxels
V1 Pre test
V1 Post test
V2V3V4 Pre test
V2V3V4 Post test

Figure S4. MVPA before and after training across visual areas.

MVPA accuracy before and after training for different voxel patterns (from 100-500 voxels) for the trained orientation presented at the trained location across layers of V1, V2, V3, V4. We observed similar learning-dependent changes in superficial layers across visual areas. Two-way repeated measures ANOVAs (ROI × session) showed a significant main effect of session for pattern size of 200 ($F(1,12) = 7.159$, $p = 0.020$), 300 ($F(1,12) = 7.751$, $p = 0.017$), 400 ($F(1,12) = 6.006$, $p = 0.031$) voxels, and a trend for pattern size of 100 ($F(1,12) = 3.743$, $p = 0.077$) and 500 ($F(1,12) = 4.587$, $p = 0.053$) voxels. We did not observe any significant ROI × session interaction (all *ps* > 0.269). Further, we did not observe any significant differences in MVPA accuracy before vs. after training in middle nor deeper layers (all *ps* > 0.539). Error bars indicate standard error of the mean across participants.